1 Magnetic dipolarizations inside geosynchronous orbit with tailward
2 ions flow

3 Xiaoying Sun[1,2], Weining William Liu [1], Suping Duan[1]

4 [1] State Key Laboratory of Space Weather, National Space Science Center (NSSC),Chinese Academy of Sciences (CAS),
5 Beijing, 100190, China
6 [2]University of Chinese Academy of Sciences, Beijing, 100049, China

7 *Correspondence to*: W .W. Liu (wliu@nssc.ac.cn), Suping Duan (spduan@nssc.ac.cn)

8 **Abstract.** Electromagnetic field and plasma data from the Time History of Events and Macroscale Interactions
9 duringSubstorms (THEMIS) near-Earth probes are used to investigate magnetic dipolarizations inside geosynchronous orbit
10 on 27 August 2014 during an intense substorm with AE_{max} ~ 1000nT. THEMIS-D (TH-D) was located inside
11 geosynchronous orbit around midnight in the interval from 09:25 UT to 09:55 UT. During this period two distinct magnetic
12 dipolarizations with tailward ions flow are observed by TH-D. The first one is displayed by magnetic elevation angle
13 increase from 15 degree to 25 degree around 09:30:40UT. The tailward perpendicular velocity is $V_{\perp x}$ ~ -50km/s. The
14 second one is presented by the elevation angle increase from 25 degree to 45 degree around 09:36 UT. And the tailward
15 perpendicular velocity is $V_{\perp x}$ ~ -70 km/s. These two significant dipolarizations are accompanied with the sharp increase in
16 the energy flux of energetic electron inside geosynchronous. After 5 min expanding of near-Earth plasma sheet (NEPS),
17 THEMIS-E (TH-E) located outside geosynchronous orbit also detects this tailward expanding plasma sheet with ion flow -
18 150 km/s. The dipolarization propagates tailward with speed -47 km/s, along 2.2 R_E distance in the X direction between
19 TH-D and TH-E within 5 min. These dipolarizations with tailward ions flow observed inside geosynchronous orbit indicate
20 new energy transfer path in the inner magnetosphere during substorms.
21 Keywords: Magnetic dipolarization, tailward ions flow, near-Earth plasma sheet, intense substorm

22 Introduction

23 Magnetic dipolarization can be observed at or inside geosynchronous orbit during intense substorms with high AE index
24 ($AE > 500$ nT) [e.g., Dai et al., 2015; Nagai, 1982; Noséet al., 2014; Ohtani et al., 2018]. Dipolarizations are marked by the
25 magneticelevation angle increase with the decrease in the radial components of B_x and B_y, and the increase in the B_z
26 component [Liu and Liang, 2009; Duan et al., 2011; Dai et al., 2014, 2015]. Ohtani et al. [2018] presented the statistics
27 characteristics of magnetic dipolarizations inside geosynchronous orbit. They reported that the dipolarization region
28 expanded in the azimuthal direction with speed 60 km/s at 5.5 R_E. Using multiple satellites conjunction observations at or

29 inside geosynchronous orbit, Dai et al. [2015] reported thatthe large dipolarization electric field was associated with

30 substorm injection of MeV electrons into the inner magnetosphere (r < 6.6 R_E).

31

32 Magnetic dipolarizations are accompanied with complex ions bulk flow in the near-Earth plasma sheet (NEPS) [e.g., Duan et

33 al., 2008; Liang et al., 2009]. Especially, it is more complex in the inner edge of NESP. Usually, the substorm-associated

34 dipolarizations in the NEPS are accompanied with earthward ions bulk flow [e.g., Angelopoulos et al., 1992; Baumjohann et

35 al., 1999; Duan et al., 2011; Liang et al., 2008; Liu et al., 2008; Nakamura et al., 2009; Shiokawa et al., 1998]. According

36 conjunction observations of THEMIS multiple probes in the NEPS, Duan et al. [2011] pointed out that the dipolarization at

37 inner edge of the near-Earth plasma sheet had no one-to-one relationship with the earthward ions bulk flow. Lui et al. [1999]

38 pointed out that dipolarization at $X \sim 10\, R_E$ was detected with tailward flow. Inside geosynchronous orbit, magnetic

39 dipolarizations were detected with earthward ions bulk flow [Dai et al., 2015].

40

41 Near-Earth Dipolarizations with low frequency waves are detected with thermal ions and electron energization [e.g., Dai et

42 al., 2015; Liang et al., 2008, 2009; Nosé et al., 2014; Ohtani et al., 2018]. These energetic particles are main source of inner

43 magnetosphere during substorms and storms. Nosé et al. [2014] proposed that the dipolarizations associated with low

44 frequency fluctuations were observed in the inner magnetosphere during the storm main phase. These low frequency

45 electromagnetic waves can accelerate O^+ ions in the perpendicular direction. The low frequency waves can accelerate

46 particles crossing the magnetic field with large perpendicular electric field [e.g., Dai et al., 2014, 2015; Duan et al., 2016;

47 Nosé et al., 2014]. Usually, Dipolarization associated dispersionless energetic particle injections is accompanied with

48 earthward ions bulk flow in the NEPS [Dai et al., 2015]. But few reports show that dipolarizations with the sharply increase

49 in the energy flux of energetic particlesassociated with tailward ions flow at or inside geosynchronous orbit.

50

51 The ballooning mode occurred in the near-Earth plasma sheet are associated with tailward expansion of plasma sheet during

52 substorms [Liu, 1997; Liu et al., 2008; Liu and Liang, 2009; Liang et al., 2009; Saito et al., 2008]. Liu et al. [2008] pointed

53 out that the ballooning mode could excite a quasi-electrostatic field a few minutes before local current disruption and that the

54 perturbations associated with ballooning instability propagated downtail.

55

56 In this paper we present a dipolarization with tailward ions flow inside geosynchronous orbit during an intense substorm

57 expansion phase. The observations in detail of an intense substorm on 27 August 2014 by TH-D and TH-E are presented in

58 section 2. Discussions and conclusions of our observation results are displayed in the last section.

59   **Observations of an intense substorm on 27 August 2014**

60   The OMNI data of the solar wind, interplanetary magnetic field (IMF) and geomagnetic field index Dst and AE during a

61   storm on August 27, 2014 are presented in Figure 1. The minimum value of Dst index is about -80 nT, as shown in Figure 1e,

62   imply that a moderate storm take placed. During the main phase of this moderate storm, there is an intense substorm with

63   the AE maximum value 1273 nT. The beginning time of this intense substorm expansion phase is around 09:31 UT with

64   decrease in the AL index. A significant substorm enhancement occur around 09:48 UT with sharply decrease in the AL index

65   and increase in the AE index.

66

67   During this intense substorm, THEMIS probes [Angelopoulos, 2008], such as TH-D and TH-E are both located in the near-

68   Earth magnetotail. Figure 2 displays the orbits of TH-D and TH-E from 09:20 to 10:00 UT in the SM coordinate system. At

69   09:30 UT, locations of these two spacecraft, are (-6.01, -0.06, 1.12) R_E for TH-D, (-8.10, -2.28, 1.92) R_E for TH-E,

70   respectively. TH-D orbit plot presents that it is located inside geosynchronous orbit at the beginning time of this intense

71   substorm expansion phase. On the other hand, TH-E is located outside geosynchronous orbit. These two spacecraft present

72   good conjunction observations during this intense substorm expansion phase. The instruments adopted in our investigations

73   are the fluxgate magnetometer (FGM) [Auster et al., 2008], the electrostatic analyzer (ESA) [McFadden et al., 2008], the

74   electric field instrument (EFI) [Bonnell et al., 2008] and the solid state telescope (SST) on board the THEMIS probes.

75

76   Figure 3 shows the plasma parameters and the electromagnetic field detected by TH-D mostly inside geosynchronous orbit at

77   about midnight section. The solar magnetic (SM) coordinate system is adopted. From top to bottom, panels are the total

78   magnetic field value, B_t and the B_x component, the B_y and B_z components, the magnetic field elevation angle defined by

79    $\theta = \tan^{-1}(B_z/(B_x{}^2 + B_y{}^2)^{1/2})$, the ion and electron density, temperature, the plasma beta value β, $\beta = 2\mu_0 nT/B^2$, which

80   determines the location of the satellite [Miyashita et al., 2000], three components of ions bulk flow velocity parallel (black

81   line) and perpendicular (red line) to the magnetic field, V_x, V_y and V_z, three components of the electric field, the E_x (red), the

82   E_y (black) and the E_z (blue), there components of convection electric field from **V**×**B**, the E_{cx} (red), the E_{cy} (black) and the

83   E_{cz} (blue), respectively. Figure 3 displays the distinct fluctuations of the magnetic field and plasma density and velocity

84   around 09:30 UT and 09:36 UT, respectively. The magnetic elevation angle has two step clear enhancements as displayed in

85   Figure 3c. The first increase in elevation angle is from about 15 degree to 25 degree during the interval from 09:30:34 UT to

86   09:30:54 UT, which are marked by the left two vertical dashed lines in Figure 3. The total magnetic field value and the B_x

87   component both decrease. The B_z component increase weakly from about 35 nT to 45 nT. The B_y component has obvious

88   fluctuations around 0 nT. These magnetic signatures indicate a magnetic dipolarization take places inside geosynchronous

89   orbit around (-6.10, -0.06, 0.43) R_E. During this weak magnetic field dipolarization, the plasma beta value, β, increases from

90   around 0.5 to 1.0. The ion and electron density and temperature both increase. Accompanied this dipolarization the tailward

91   ions bulk flow, $V_{//x} \sim -100 km/s$ and the perpendicular component to the magnetic field in the X direction, $V_{\perp x} \sim -50\ km/s$

92   is detected by TH-D, as shown in Figure 3g. The perpendicular velocity in the Y direction is mainly dawnward at the

93   beginning time of this dipolarization, $V_{\perp y}$ ~ -30km/s. The electric field detected by TH-D also has large fluctuations with

94   negative E_y value during the first depolarization as shown in Figure 3j. During the intervals from 09:30:34 UT to 09:30:54

95   UT the convection electric field direction is dawnward with large magnitude, E_{cy} ~ -12 mV/m, as presented in Figure 3k.

96   The second magnetic field elevation angle increases sharply at around 09:36 as displayed in Figure 3c marked by the right

97   two vertical dashed lines. The elevation angle increases from about 25 degree to 45 degree during the interval from 09:36:06

98   UT to 09:36:21UT. The magnetic field has similar variations to the first dipolarization signatures. Especially, the second

99   dipolarization has larger elevation angle maximum value, ~ 45 degree, as marked by the fourth vertical dashed line in Figure

100   3c. During the second dipolarization the tailward ions bulk flow perpendicular to the magnetic field is also detected by TH-D,

101   $V_{\perp x}$ ~ -70 km/s, as presented in Figure 3g. Also the significant negative E_y component is companied by this intense

102   dipolarization in Figure 3j and 3k.

103

104   Duringthe intervals of magnetic dipolarizations with tailward ions bulk flow detected by TH-D inside geosynchronous orbit,

105   TH-E observed very weak increase in the magnetic field elevation angle and the B_z component around 09:35 UT and 09:41

106   UT, as shown in Figure 4b and 4c, about 5 min after two dipolarizations detected by TH-D. The ions and electrondensity

107   andtemperature increase weakly from very low value as displayed in Figure 4d and 4e. Outside geosynchronous orbit, TH-E

108   observed very low beta value, as shown in Figure 4f, β ~ 0.01 and β ~ 0.2 around 09:35 UT and 09:41 UT, respectively.

109   Interesting phenomena that the weak dipolarization was with the tailward ions bulk flow, $V_{//x}$ ~ -180km/s, is also detected

110   by TH-E around 09:35 UT as shown in Figure 4g. The perpendicular velocity is dominated in the negative Y direction, $V_{\perp y}$ ~

111   -50 km/s.

112

113   Associated with the intense electric field observed by TH-D inside geosynchronous orbitduring this two dipolarizations, the

114   energy fluxes of energetic electrons, as shown in the second panel of Figure 5, with energy of 31 keV(blue), 41 keV (gray),

115   52 keV (red), 65.5 keV (black), 93 keV(brown) and 139 keV (purple) all simultaneously increase at 09:30:38 UT and

116   09:36:09UT detected by SST/TH-D, respectively. These energetic electrons have quasi-perpendicular pitch angle

117   distribution, as presented in the bottom panel of Figure 5.

118   **Discussion and conclusions**

119   The dipolarizations with tailward ions bulk flow inside geosynchronous orbit are investigated in our present paper.

120   Accompanied these dipolarizations the energy fluxes of energetic electrons with energy between 31 keV and 139 keV

121   simultaneously increase inside geosynchronous orbit. According to these energetic electrons pitch angle distributions, it is

122   found that high energy electrons mainly in the quasi-perpendicular direction to the magnetic field, as shown in Figure 5. On

123 the other hand, the inductive electric field during these two magneticdipolarization is in the dawnward direction as display in

124 Figure 3j and 3k. Previous research work reported that the inductive electric field associated with substorm dipolarization

125 can accelerate particles in the near-Earth plasma sheet [Dai et al., 2014, 2015; Duan et al., 2016; Fu et al., 2011; Fok et al.,

126 2001; Liu et al., 2010; Lui et al., 1988, 1999; Nakamura et al., 2009; Nosé et al., 2014]. As shown in Figure 3j around

127 09:36:30 UT the inductive electric fields in the second dipolarization are dominated in the E_y component with large negative

128 value, E_y ~ $-25mV/m$, and the X component also increase with negative value E_x ~ $-6mV/m$. This intense electric field can

129 drive ions moving into the tailward-dawnward direction. On the other hand, we can calculate the energy quantity relationship

130 between the electric field and energetic electrons. Estimating the energy of such intense E_y in the distance of ~1000 km is

131 about ~ 10^{-15} Joule. The energetic electrons with energy range from 31 keV to 139 keV are in the same energy order ~10^{-15}

132 ^{15}Joule. It is inferred that the intense E_y can perpendicularly accelerate electrons to tens keV state.

133

134 Dipolarizations occurring at the inner edge of plasma sheet are complicated with disturbances of ions bulk flow and

135 electromagnetic field. Lui et al. [1999] pointed out that near-Earth dipolarization was a non-MHD process and was also

136 accompanied with tailward ions flow.Our observations of dipolarizations inside geosynchronous orbit are also associated

137 with tailward ions flow. This result is consistent with the report proposed by Liu et al. [2008] that the perturbations

138 associated with the ballooning mode in the near-Earth plasma sheet propagating tailward. Based on the statistic studies, Nosé

139 et al. [2016] proposed that the occurrence probability of the dipolarizations in the inner magnetosphere had a peak at 21:00-

140 00:00 MLT. Our observations show that two distinct dipolarizations with tailward flow inside geosynchronous orbit are

141 detected by TH-D around 00:02 MLT and 00:05 MLT, respectively.

142

143 According to the distance between TH-D and TH-E, (-2.23, -2.30, 0.56)R_E, and the delay time of dipolarization from inside

144 to outside geosynchronous orbit, ~5 min, the dipolarization propagating speed or the plasma sheet expanding speed can be

145 estimated as V_x ~ $-47\ km/s$, V_y ~ $-48\ km/s$, V_z ~ $12\ km/s$, respectively. Liou et al. [2002] proposed that the dipolarization

146 region expanding speed was ~ $60\ km/s$ westward at geosynchronous. Comparing observations between TH-D and TH-E in

147 our investigations, the azimuth speed of dipolarization region is obtained ~ $48\ km/s$. These two observational results are

148 consistent with each other.

149

150 Based on the above observation analysis, we can draw the results as following. Two distinct magnetic dipolarizations with

151 tailward ions flow are observed by TH-D inside geosynchronous orbit on 27 August 2014 during the intense substorm with

152 AE_{max} ~ 1000nT. TH-D was located inside geosynchronous orbit around midnight in the interval from 09:20 UT to 10:00

153 UT. The first dipolarization is displayed by magnetic elevation angle increase from 15 degree to 25 degree around

154 09:30:40UT. The second one is presented by the elevation angle increase from 25 degree to 45 degree around 09:36 UT.

155 These two significant dipolarizations are accompanied with the energy flux of energetic electrons simultaneously increase

156 inside geosynchronous orbit. After 5 min expanding tailward of near-Earth plasma sheet, TH-E located outside

157 geosynchronous orbit also detects this tailward expanding plasma sheet with ion flow -150 km/s. The dipolarization

158 propagates tailward with speed -45 km/s, along 2 R_E distant in the X direction between TH-D and TH-E within 5 min.

159 These dipolarizations with tailward ion flow observed inside geosynchronous orbit indicate new energy transfer path in the

160 inner magnetosphere during substorms.

Acknowledgments

References

171

172 Angelopoulos, V.: The THEMIS Mission, Space Science Reviews, 141, 5-34, 2008.

173 Angelopoulos, V., Baumjohann, W., Kennel, C. F., Coroniti, F. V., Kivelson, M. G., Pellat, R., Walker, R. J., Lühr, H., and

174 Paschmann, G.: Bursty bulk flows in the inner central plasma sheet, Journal of Geophysical Research, 97, 4027, 1992.

175 Auster, H. U., Glassmeier, K. H., Magnes, W., Aydogar, O., Baumjohann, W., Constantinescu, D., Fischer, D., Fornacon, K.

176 H., Georgescu, E., Harvey, P., Hillenmaier, O., Kroth, R., Ludlam, M., Narita, Y., Nakamura, R., Okrafka, K., Plaschke, F.,

177 Richter, I., Schwarzl, H., Stoll, B., Valavanoglou, A., and Wiedemann, M.: The THEMIS Fluxgate Magnetometer, Space

178 Science Reviews, 141, 235-264, 2008.

179 Baumjohann, W., Hesse, M., Kokubun, S., Mukai, T., Nagai, T., and Petrukovich, A. A.: Substorm dipolarization and

180 recovery, Journal of Geophysical Research: Space Physics, 104, 24995-25000, 1999.

181 Bonnell, J. W., Mozer, F. S., Delory, G. T., Hull, A. J., Ergun, R. E., Cully, C. M., Angelopoulos, V., and Harvey, P. R.: The

182 Electric Field Instrument (EFI) for THEMIS, Space Science Reviews, 141, 303-341, 2008.

183 Dai, L., Wang, C., Duan, S., He, Z., Wygant, J. R., Cattell, C. A., Tao, X., Su, Z., Kletzing, C., Baker, D. N., Li, X.,

184 Malaspina, D., Blake, J. B., Fennell, J., Claudepierre, S., Turner, D. L., Reeves, G. D., Funsten, H. O., Spence, H. E.,

185   Angelopoulos, V., Fruehauff, D., Chen, L., Thaller, S., Breneman, A., and Tang, X.: Near-Earth injection of MeV electrons

186   associated with intense dipolarization electric fields: Van Allen Probes observations, Geophys Res Lett, 42, 6170-6179, 2015.

187   Dai, L., Wygant, J. R., Cattell, C. A., Thaller, S., Kersten, K., Breneman, A., Tang, X., Friedel, R. H., Claudepierre, S. G.,

188   and Tao, X.: Evidence for injection of relativistic electrons into the Earth's outer radiation belt via intense substorm electric

189   fields, Geophysical Research Letters, 41, 1133-1141, 2014.

190   Duan, S., Liu, Z., Cao, J., Lu, L., Rème, H., Dandouras, I., and Carr, C. M.: TC-1 observation of ion high-speed flow

191   reversal in the near-Earth plasma sheet during substorm, Science in China Series E: Technological Sciences, 51, 1721-1730,

192   2008.

193   Duan, S. P., Dai, L., Wang, C., Liang, J., Lui, A. T. Y., Chen, L. J., He, Z. H., Zhang, Y. C., and Angelopoulos, V.: Evidence

194   of kinetic Alfven eigenmode in the near-Earth magnetotail during substorm expansion phase, Journal of Geophysical

195   Research-Space Physics, 121, 4316-4330, 2016.

196   Duan, S. P., Liu, Z. X., Liang, J., Zhang, Y. C., and Chen, T.: Multiple magnetic dipolarizations observed by THEMIS

197   during a substorm, Annales Geophysicae, 29, 331-339, 2011.

198   Fok, M.-C., Moore, T. E., and Spjeldvik, W. N.: Rapid enhancement of radiation belt electron fluxes due to substorm

199   dipolarization of the geomagnetic field, Journal of Geophysical Research: Space Physics, 106, 3873-3881, 2001.

200   Fu, H. S., Khotyaintsev, Y. V., André, M., and Vaivads, A.: Fermi and betatron acceleration of suprathermal electrons

201   behind dipolarization fronts, Geophysical Research Letters, 38, n/a-n/a, 2011.

202   Liang, J., Donovan, E. F., Liu, W. W., Jackel, B., Syrjäsuo, M., Mende, S. B., Frey, H. U., Angelopoulos, V., and Connors,

203   M.: Intensification of preexisting auroral arc at substorm expansion phase onset: Wave-like disruption during the first tens of

204   seconds, Geophysical Research Letters, 35, 2008.

205   Liang, J., Liu, W. W., and Donovan, E. F.: Ion temperature drop and quasi-electrostatic electric field at the current sheet

206   boundary minutes prior to the local current disruption, Journal of Geophysical Research: Space Physics, 114, n/a-n/a, 2009.

207   Liou, K., Meng, C.-I., Lui, A. T. Y., Newell, P. T., and Wing, S.: Magnetic dipolarization with substorm expansion onset,

208   Journal of Geophysical Research, 107, 2002.

209   Liu, W. W.: Physics of the explosive growth phase: Ballooning instability revisited, Journal of Geophysical Research: Space

210   Physics, 102, 4927-4931, 1997.

211   Liu, W. W. and Liang, J.: Disruption of magnetospheric current sheet by quasi-electrostatic field in the substorm expansion

212   phase, Annales Geophysicae, 27, 1941-1950, 2009.

213   Liu, W. W., Liang, J., and Donovan, E. F.: Electrostatic field and ion temperature drop in thin current sheets: A theory,

214   Journal of Geophysical Research: Space Physics, 115, n/a-n/a, 2010.

215   Liu, W. W., Liang, J., and Donovan, E. F.: Interaction between kinetic ballooning perturbation and thin current sheet: Quasi-

216   electrostatic field, local onset, and global characteristics, Geophysical Research Letters, 35, 2008.

217   Lui, A. T. Y., Liou, K., Nosé, M., Ohtani, S., Williams, D. J., Mukai, T., Tsuruda, K., and Kokubun, S.: Near-Earth

218   dipolarization: Evidence for a non-MHD process, Geophysical Research Letters, 26, 2905-2908, 1999.

219 Lui, A. T. Y., Lopez, R. E., Krimigis, S. M., McEntire, R. W., Zanetti, L. J., and Potemra, T. A.: A case study of magnetotail

220 current sheet disruption and diversion, Geophysical Research Letters, 15, 721-724, 1988.

221 McFadden, J. P., Carlson, C. W., Larson, D., Ludlam, M., Abiad, R., Elliott, B., Turin, P., Marckwordt, M., and

222 Angelopoulos, V.: The THEMIS ESA Plasma Instrument and In-flight Calibration, Space Science Reviews, 141, 277-302,

223 2008.

224 Miyashita, Y., Machida, S., Mukai, T., Saito, Y., Tsuruda, K., Hayakawa, H., and Sutcliffe, P. R.: A statistical study of

225 variations in the near and middistant magnetotail associated with substorm onsets: GEOTAIL observations, Journal of

226 Geophysical Research: Space Physics, 105, 15913-15930, 2000.

227 Nagai, T.: Observed magnetic substorm signatures at synchronous altitude, Journal of Geophysical Research, 87, 4405, 1982.

228 Nakamura, R., Retino, A., Baumjohann, W., Volwerk, M., Erkaev, N., Klecker, B., Lucek, E. A., Dandouras, I., Andre, M.,

229 and Khotyaintsev, Y.: Evolution of dipolarization in the near-Earth current sheet induced by Earthward rapid flux transport,

230 Annales Geophysicae, 27, 1743-1754, 2009.

231 Nosé, M., Keika, K., Kletzing, C. A., Spence, H. E., Smith, C. W., MacDowall, R. J., Reeves, G. D., Larsen, B. A., and

232 Mitchell, D. G.: Van Allen Probes observations of magnetic field dipolarization and its associated O+ flux variations in the

233 inner magnetosphere at L < 6.6, Journal of Geophysical Research-Space Physics, 121, 7572-7589, 2016.

234 Nosé, M., Takahashi, K., Keika, K., Kistler, L. M., Koga, K., Koshiishi, H., Matsumoto, H., Shoji, M., Miyashita, Y., and

235 Nomura, R.: Magnetic fluctuations embedded in dipolarization inside geosynchronous orbit and their associated selective

236 acceleration of O+ ions, Journal of Geophysical Research: Space Physics, 119, 4639-4655, 2014.

237 Ohtani, S., Motoba, T., Gkioulidou, M., Takahashi, K., and Singer, H. J.: Spatial Development of the Dipolarization Region

238 in the Inner Magnetosphere, Journal of Geophysical Research: Space Physics, 123, 5452-5463, 2018.

239 Saito, M. H., Miyashita, Y., Fujimoto, M., Shinohara, I., Saito, Y., Liou, K., and Mukai, T.: Ballooning mode waves prior to

240 substorm-associated dipolarizations: Geotail observations, Geophysical Research Letters, 35, n/a-n/a, 2008.

241 Shiokawa, K., Baumjohann, W., Haerendel, G., Paschmann, G., Fennell, J. F., Friis-Christensen, E., Lühr, H., Reeves, G. D.,

242 Russell, C. T., Sutcliffe, P. R., and Takahashi, K.: High-speed ion flow, substorm current wedge, and multiple Pi 2

243 pulsations, Journal of Geophysical Research: Space Physics, 103, 4491-4507, 1998.

244

245

246 Figure 1 The solar wind, IMF B_z conditions and geomagnetic indices between 01:00 UT and 23:00 UT on August 27, 2014. From top to
247 bottom of (a ~ g) panels show the change of solar wind dynamic pressure (a), $B_{z,IMF}$ in GSM coordinate (b), the x component of the solar
248 wind flow speedin GSM coordinate (c), electric field$E$ (d), *AE/AU/AL* index (e),*SYM-H* indices (f), and *ASY-H* index (g). From left to right,
249 the verticaldotted lines in (a ~ g) panels marked the time 01:48 UT, 06:42 UT, 09:31 UT, 09:48 UT, 21:56 UT and 22:35 UT, respectively.

250

251 Figure 2 The orbits of TH-D and TH-E in the $X - Y_{SM}$ plane and the $X - Z_{SM}$ plane from 09:20 to 10:00 UT on 27 August 2014, which
252 were in the nightside magnetosphere. The arrow shows the flying direction of the satellites. TH-D is redand TH-E is blue.

253

254 Figure 3 The electromagnetic field and plasma parameters detected by TH-D in the intervals from 09:25 UT to 09:55 UT on August 27,
255 2014. The Solar Magnetic (SM)coordinated system is adopted. From top to bottom, panels showed that (a)the total magnetic field B_t
256 (black) and the X component B_x (red), (b) the Y component B_y (green) and the Z component B_z (blue), (c)the magnetic field elevation
257 angle θ; (d) ion and electron density N_i, N_e; (e)ion and electron temperature T_i, T_e; (f) plasma beta β; (g) the X component of ion
258 parallelvelocity and perpendicular velocity V_{parx}, V_{perpx}; (h) the Y component of ion parallel velocity and perpendicularvelocity
259 V_{pary}, V_{perpy}; (i) the Z component of ion parallel velocity and perpendicular velocity V_{parz}, V_{perpz}; (j) the electric field E_x (red), E_y
260 (black), and E_z (blue) by assuming $\mathbf{E} \cdot \mathbf{B} = 0$; (k) the electric field E_{cx} (red), E_{cy} (black), E_{cz} (blue) calculated by $\mathbf{E} = \mathbf{B} \times \mathbf{V}$. The black
261 vertical dashed lines marked the time 09:30:34 UT,09:30:54UT, 09:36:06 UT and 09:36:21 UT, respectively.

262

263 Figure 4 The electromagnetic field and plasma parameters detected by TH-E in the intervals from 09:25 UT to 09:55 UT on August 27,
264 2014.The Figure format is the same as Figure 3.The black vertical dashed lines marked the time 09:35:36 UT and 09:36:18 UT.
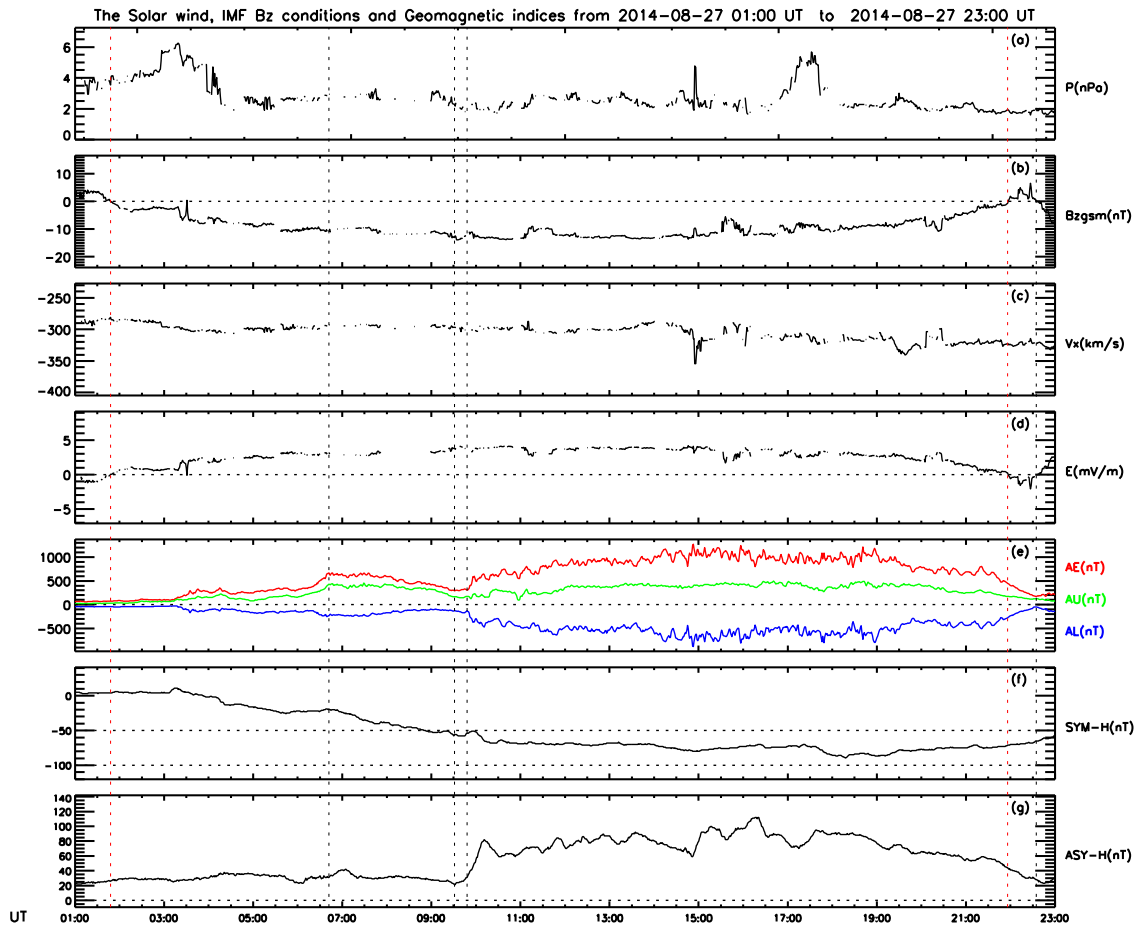
265

266 Figure 5 The energy flux and pitch angle distribution of energetic electrons detected by SST/TH-D in 3 second time resolution. The red
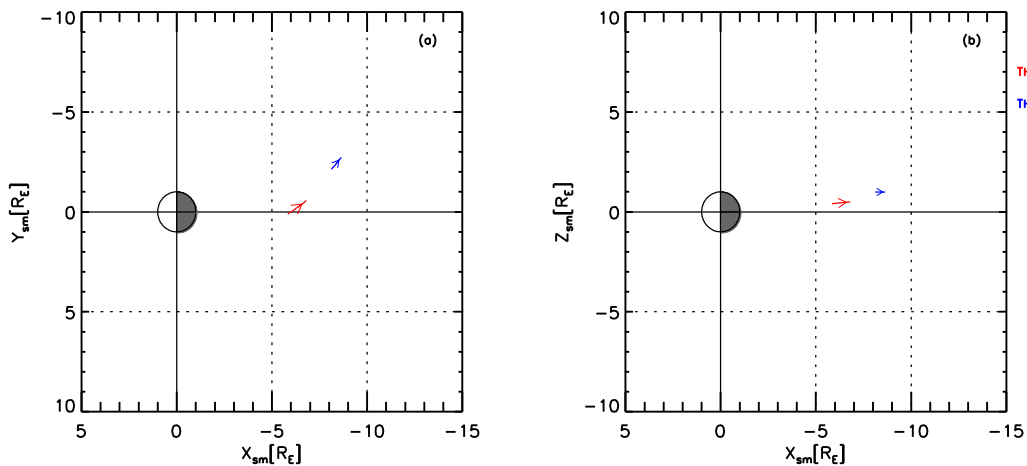267 vertical lines marked the time 09:30:38 UT and 09:36:09 UT.
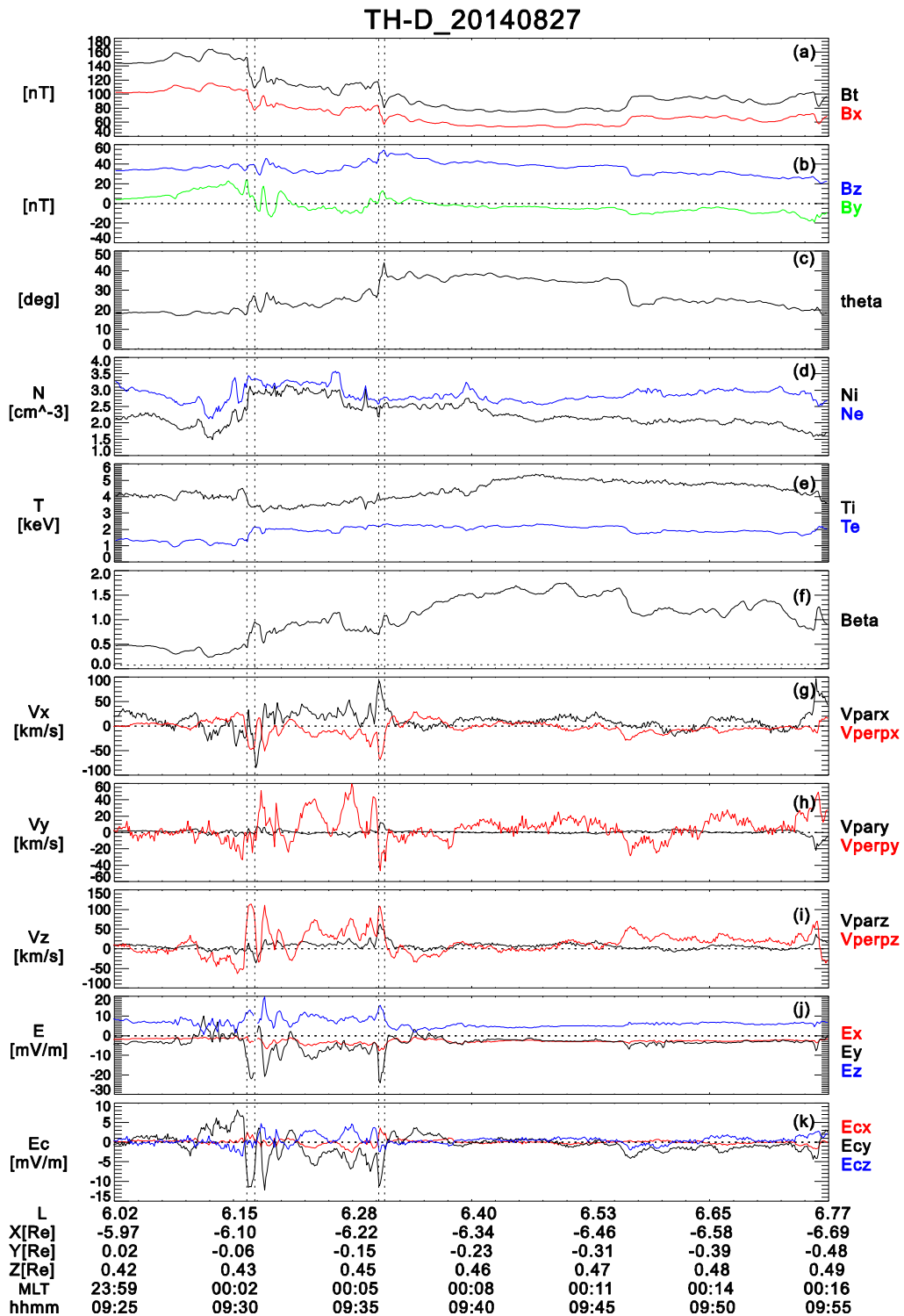
268

269   Figure 1

270

271   Figure 2

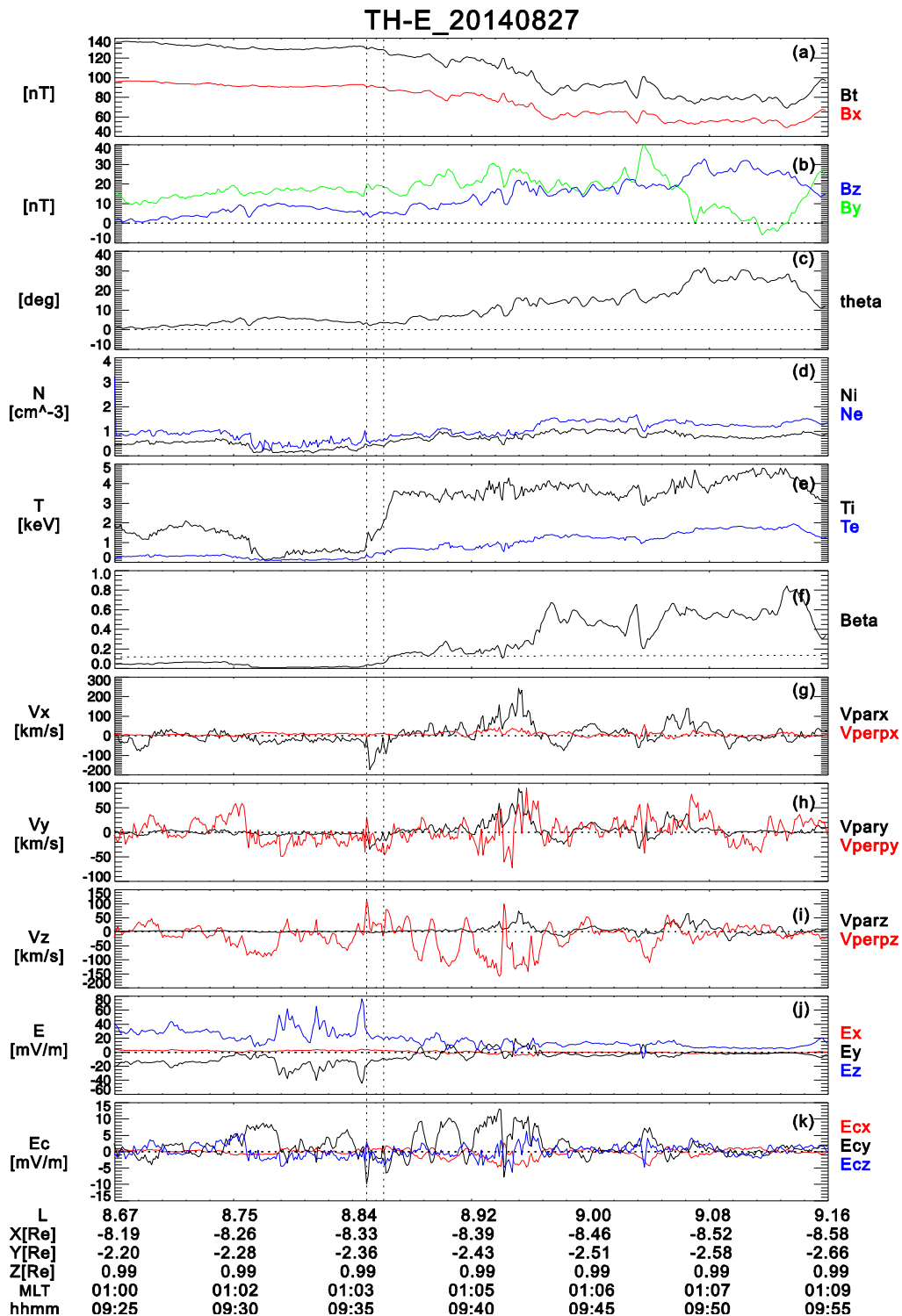The orbit of TH-D and TH-E during 2014-08-27 storm (09:20 ~ 10:00 UT)
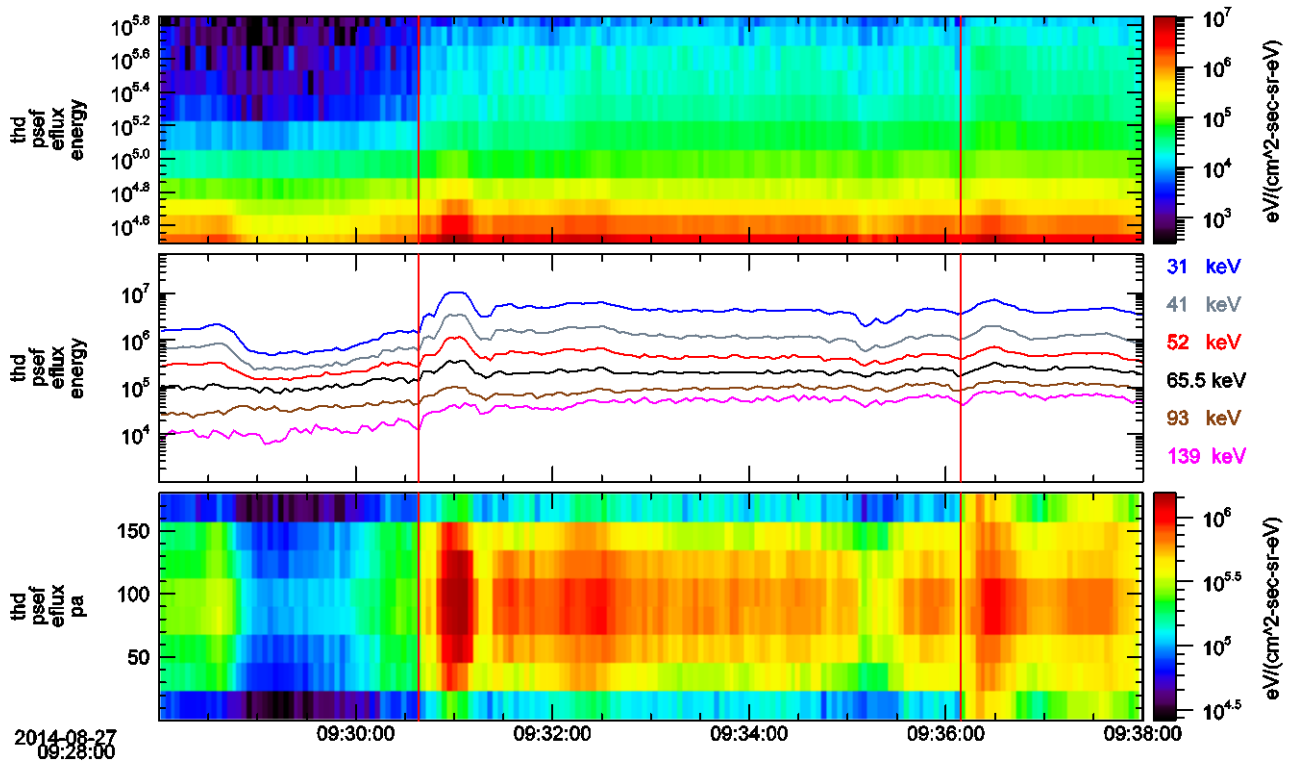
272

Annales
Geophysicae
Discussions

273   Figure 3

274

275   Figure 4

276

277   Figure 5

278

279